AI Foundation Models Facilitate Real-time Global GNSS Precipitable Water Vapor Retrieval with Sub-millimeter Accuracy

Junsheng Ding[1], Wu Chen[1], Junping Chen[2,3], Jungang Wang[4,5], Yize Zhang[2], Duojie Weng[1], Tong Liu[1], Xiaolong Mi[1], Benedikt Soja[6], and Lei Bai[7]

[1]Department of Land Surveying and Geo-Informatics, The Hong Kong Polytechnic University
[2]Shanghai Astronomical Observatory, Chinese Academy of Sciences
[3]School of Astronomy and Space Science, University of Chinese Academy of Sciences
[4]Department of Geodesy, GeoForschungsZentrum (GFZ)
[5]Institut für Geodäsie und Geoinformationstechnik, Technische Universität Berlin
[6]Institute of Geodesy and Photogrammetry, ETH Zurich
[7]Shanghai AI Laboratory

July 12, 2024

Abstract

Currently, over 20,000 Global Navigation Satellite Systems (GNSS) stations are installed worldwide to provide tropospheric delay products with high-quality and high temporal resolution (5 min). However, few of these stations are equipped with on-site meteorological sensors, leading to the challenge of the real-time transformation of this tropospheric delay into accurate precipitable water vapor (PWV). We propose a real-time high-accuracy GNSS PWV retrieval method based on artificial intelligence weather forecast foundation models. This innovative approach efficiently calculates integral zenith hydrostatic delay (ZHD) and integral weighted mean temperature (Tm) at any global location locally within seconds, bypassing inaccuracies inherent in empirical ZHD and Tm models, significantly reducing PWV errors. The method is evaluated on three representative foundation models, Pangu-Weather, GraphCast, and FengWu, showing precision loss of PWV below 0.1 mm using 6-hour forecasts. It offers a robust solution for instantaneous GNSS PWV retrieval and enhances global hazardous weather monitoring and alert systems.

AI Foundation Models Facilitate Real-time Global GNSS Precipitable Water Vapor Retrieval with Sub-millimeter Accuracy

Junsheng Ding[1], Wu Chen[1], Junping Chen[2,3,*], Jungang Wang[4,5], Yize Zhang[2], Duojie Weng[1], Tong Liu[1], Xiaolong Mi[1], Benedikt Soja[6], Lei Bai[7]

[1] Department of Land Surveying and Geo-Informatics, The Hong Kong Polytechnic University, Hong Kong, China;
[2] Shanghai Astronomical Observatory, Chinese Academy of Sciences, Shanghai, China;
[3] School of Astronomy and Space Science, University of Chinese Academy of Sciences, Beijing, China;
[4] Department of Geodesy, GeoForschungsZentrum (GFZ), Potsdam, Germany;
[5] Technische Universität Berlin, Institut für Geodäsie und Geoinformationstechnik, Berlin, Germany;
[6] Institute of Geodesy and Photogrammetry, ETH Zurich, Zurich, Switzerland;
[7] Shanghai AI Laboratory, Shanghai, China.

Corresponding Author: Junping Chen, E-mail: junping@shao.ac.cn

Key Points:

- Proposes real-time GNSS PWV retrieval method based on weather forecast foundation models represented by Pangu-Weather, GraphCast and FengWu
- Generates integral ZHD and Tm at any global position locally within seconds, circumventing inaccuracies inherent in empirical ZHD and Tm models
- On a global scale, the PWV error introduced by ZHD and Tm using the 6-hour forecast under the new method is less than 0.1 mm

Abstract

Currently, over 20,000 Global Navigation Satellite Systems (GNSS) stations are installed worldwide to provide tropospheric delay products with high-quality and high temporal resolution (5 min). However, few of these stations are equipped with on-site meteorological sensors, leading to the challenge of the real-time transformation of this tropospheric delay into accurate precipitable water vapor (PWV). We propose a real-time high-accuracy GNSS PWV retrieval method based on artificial intelligence weather forecast foundation models. This innovative approach efficiently calculates integral zenith hydrostatic delay (ZHD) and integral weighted mean temperature (Tm) at any global location locally within seconds, bypassing inaccuracies inherent in empirical ZHD and Tm models, significantly reducing PWV errors. The method is evaluated on three representative foundation models, Pangu-Weather, GraphCast, and FengWu, showing precision loss of PWV below 0.1 mm using 6-hour forecasts. It offers a robust solution for instantaneous GNSS PWV retrieval and enhances global hazardous weather monitoring and alert systems.

Plain Language Summary

The tropospheric delay products can be provided at over 20,000 Global Navigation Satellite Systems (GNSS) stations worldwide. The products can be converted into highly accurate and high-quality precipitable water vapor (PWV), which is crucial for understanding global water and energy cycles, as well as for meteorological and climatic studies. However, the conversion of GNSS zenith total delay (ZTD) into PWV relies on two key factors: zenith hydrostatic delay (ZHD) and weighted mean temperature (Tm), typically provided by co-located radiosondes. Unfortunately, the majority of GNSS stations do not meet this requirement. Recent progress in artificial intelligence (AI) provides us new opportunities to address this challenge. We propose a real-time GNSS PWV retrieval method based on AI weather forecast foundation models (i.e. Pangu-Weather, GraphCast, and FengWu), from which ZHD and Tm are obtained to transform GNSS ZTD into PWV. This approach effectively avoids introducing empirical model errors into the PWV by locally generating forecasted integrated ZHD and Tm for any global location within seconds. The PWV error introduced using 6-hour forecast results is less than 0.1 mm. This study offers a crucial solution for real-time GNSS PWV inversion, which will be valuable for monitoring and providing early warnings of meteorological hazards worldwide.

1. Introduction

Precipitable water vapor (PWV) is the primary greenhouse gas and an integral part of the climate and weather system, influencing the global water and energy cycles (*Rocken et al., 1997; Wang et al., 2007; Adams et al., 2023; Ding et al., 2022a*). The transport and dissipation of PWV are affected by several ecological and meteorological factors such as vegetation cover, topography (*Yu et al., 2017*), drought

(*Wang et al., 2018*) and temperature (*Ma et al., 2022*), which leads to its high variability in time and space (*Jiang et al., 2024*). Accurate PWV measurements have been a major challenge (*Zheng et al., 2022*). The derivation of PWV from Global Navigation Satellite Systems (GNSS) stands out as an increasingly promising approach due to its low cost, high temporal resolution, all-weather observational capability (*Ding et al., 2017; Miranda et al., 2023*), and the consistent delivery of PWV with high accuracy and data integrity (*Vaquero-Martínez et al., 2019; Ding et al., 2022b*). GNSS-driven PWVs have been widely used for monitoring and prediction of hurricane tracks (*Ejigu et al., 2021*), responding to thermal anomalies after the earthquake (*Guo et al., 2023*), forecasting and monitoring heavy rainfall (*Huang et al., 2021; Zhao et al., 2020*) and unveiling the characteristics of extreme drought and wetness events (*Zhu et al., 2024*).

However, the PWV could not be obtained directly by GNSS measurements. It can be estimated through two steps: (1) the zenith hydrostatic delay (ZHD) is subtracted from the zenith total delay (ZTD) to obtain a clean zenith wet delay (ZWD); and (2) the ZWD is converted to PWV by multiplying it by a conversion factor, which is determined by the weighted average temperature (Tm). Therefore, the PWV error is affected by the ZHD and Tm errors. The incorrect ZHD and Tm will lead to PWV errors of several millimeters (*Yuan et al., 2014; Li et al., 2018; Ding et al., 2023*) and may lead to negative computed GNSS PWVs at high altitudes where water vapor is thin, as well as in polar regions (*Yuan et al., 2023*). Furthermore, the great majority of GNSS stations are not equipped with meteorological sensors, and even those that have sensors can only gather data from the surface, which is insufficient to meet the requirements of the vertical integration method for determining ZHD and Tm in real time. As a result, they are forced to use an empirical model, which absorbs the PWV in the empirical model error, to settle for less-than-ideal results. *Zheng et al., (2022)* attempted to replace the ZTD to PWV transformation by machine learning, and they obtained better results than the traditional empirical model (using ERA5 as a reference, the RMSE of PWV decreased from 2.8 mm in the GPT3 results to 2.4 mm). However, it is still actually an empirical model, which accuracy improvement may not satisfy the need for high-accuracy water vapor monitoring and acquisition. Therefore, in the traditional method, either post-processing is used to obtain meteorological data by reanalyzed data for GNSS PWV computation, or GNSS stations are co-located with radiosonde sites to obtain the atmospheric vertical profile data for GNSS PWV retrieval. The former cannot be done in real-time, and the latter is nearly impossible to achieve for special environments, such as shipboard GNSS PWV retrieval at sea (*Wang et al., 2019; Wei et al., 2023; Wu et al., 2023*). Furthermore, traditional NWM (Numerical Weather Model) forecasts (such as ECMWF IFS, NCEP GFS, etc.) can also help with real-time GNSS PWV acquisition. Nevertheless, as this component normally requires authorization for usage and depends on major meteorological agencies for generation and does not support local inference, it is not included in the framework of this research.

In this contribution, we aim at providing high-accuracy and real-time GNSS PWV with global coverage while minimizing the errors caused by inaccuracy ZHD and Tm. We present a new method to acquire forecasted ZHD and Tm via AI weather forecast foundation models such as Pangu-Weather, GraphCast and FengWu. By using this new method, empirical modeling errors can be minimized. Notably, the computations can be performed on any user's local device, with global results achievable within seconds. This paper is organized as follows. Section 2 describes GNSS tropospheric delay data set and radiosonde data set, along with describing the method of converting GNSS ZTD to PWV. Section 3 evaluates the performance of the proposed method. Section 4 summarizes and presents our conclusions.

2. Methods and Data

The high-accuracy GNSS PWV depends on the high-accuracy ZHD and Tm parameters. In this study, these parameters will be derived from AI weather forecast foundation models. In this section, we first outline the streamlined computational process for real-time GNSS PWV retrieval. Then we introduce three representative foundation models used in our experiments: Pangu-Weather, GraphCast, and FengWu, and give the flowchart under this new method. Finally, the GNSS tropospheric products and radiosonde data of 2022 that serve to assess the accuracy are described.

2.1. PWV Retrieval from GNSS Tropospheric Delays

The high-precision ZWD is first obtained by subtracting the high-precision ZHD from the GNSS ZTD (*Jade et al., 2008*):

$$ZWD = ZTD - ZHD \tag{1}$$

The ZHD is defined as the integral of the refractive index along the path in the zenith direction and is calculated as follows:

$$ZHD = 10^{-6}\int_{H_s}^{\infty} N_h(z)\mathrm{d}z = \sum_{H_s}^{H_{top}}\left[\left(n_{h,i}-1\right)\Delta H_i\right] \tag{2}$$

Where H_s and H_{top} are the height of the station (surface) and the top of the troposphere, respectively. However, the calculation of the hydrostatic refraction index requires measurements of air pressure and temperature in a vertical profile, which are difficult to obtain. A more common approach is to compute the ZHD through the following Saastamoinen model (*Saastamoinen 1972*):

$$ZHD = 2.2768\cdot\frac{P_s}{1-2.66\times10^{-3}\cdot\cos\left(2\varphi_s\right)-2.8\times10^{-7}h_s} \tag{3}$$

Where P_s, φ_s and h_s are pressure, latitude and height of station locations. The Saastamoinen model, requiring mainly surface pressure due to the fixed latitude and height at a station, delivers millimeter-accurate ZHDs and is widely adopted for its simplicity and effectiveness.

After obtaining the ZWD, the GNSS PWV can be calculated by the following equations:

$$\mathrm{PWV} = \Pi\cdot\mathrm{ZWD} \tag{4}$$

$$\Pi = \frac{10^6}{R_w\cdot\left[k_2-\varepsilon k_1+k_3/T_m\right]} \tag{5}$$

Where Π is the conversion factor, and $\varepsilon = M_w/M_d$, $R_w = R/M_w$ with the universal gas constant R; M_w and M_d are molar weight of water vapor and dry constituents, respectively; k_1, k_2 and k_3 are the "Rueger - best average" values, which are 77.6890 K/hPa, 71.2952 K/hPa and 375463 K^2/hPa respectively. In Eq. (5), all variables are constants except for the weighted average temperature T_m. T_m is defined as:

$$T_{\mathrm{m}} = \frac{\int_{H_s}^{\infty}(\frac{e}{T})\,\mathrm{d}z}{\int_{H_s}^{\infty}(\frac{e}{T^2})\,\mathrm{d}z} = \frac{\sum_{H_{\mathrm{s}}}^{H_{\mathrm{top}}}\frac{e_j}{T_j}\Delta H_j}{\sum_{H_{\mathrm{s}}}^{H_{\mathrm{top}}}\frac{e_j}{T_j^2}\Delta H_j}, \tag{6}$$

where e and T are water vapor pressure (in hPa) and temperature (in K) profiles from station height H_s to the top of the troposphere. Similar to ZHD computation, the Bevis model (*Bevis et al., 1992*) is commonly employed for Tm’s calculation due to the difficulty in obtaining vertical profiles of temperature and vapor pressure. This empirical model offers a practical alternative when detailed atmospheric data is scarce.

$$T_{\mathrm{m}} = 70.2 + 0.72 \cdot T_{\mathrm{s}} \tag{7}$$

where T_s is the surface temperature at the site location. Note that in the integration method mentioned above (Eq. 2 and Eq. 6), the top of the tropopause does not correspond to the topmost pressure level of the NWM model (i.e. 1 hPa for ERA5). Instead, a reasonable extrapolation is performed as described in *Hofmeister, 2016* for relevant vertical and horizontal interpolation methods. Note the empirical models mentioned in this paper refer to the Saastamoinen and Bevis models (Eq. 3 and Eq. 7).

2.2. AI Weather Forecast Foundation Models

Pangu-Weather, developed by Huawei Cloud, is the first AI weather forecast foundation model to exceed the accuracy of traditional numerical forecasting methods (operational IFS) for medium- and long-term weather forecasts (*Bi et al., 2023*). It is constructed based on a 3D Earth-Specific Transformer (3DEST), which can handle complex 3D meteorological data well and reduce iteration error (*Bi et al., 2023*). GraphCast, proposed by Google DeepMind, is a state-of-the-art (SOTA) weather forecasting foundation model based on graph neural networks (GNN) technology. Its "encode-process-decode" modeling structure exhibits excellent performance, outperforming Pangu-Weather on 99.2% of its targets (*Lam et al., 2023*). FengWu, proposed by the Shanghai Artificial Intelligence Laboratory, is another advanced weather forecast foundation model. FengWu is based on multi-modal and multi-task deep learning methods and performs better than GraphCast in predicting 80% of the 880 reported predictands (*Chen et al., 2023*). Pangu-Weather and GraphCast are online as part of ECMWF's operational suite, and everyone can benefit from their 10-day global weather forecasts without running code. Note that Pangu-Weather only supports 13 layers of pressure level inference, while GraphCast and FengWu support up to 37 layers. The foundation models employ a "roll back" method of forecasting, wherein the input to each forecast is the output of its previous forecast. We employ a minimum forecasting step of 6 hours in this experiment, and every forecast time is a multiple of 6 hours. As of March 2024, additional AI models like ClimaX, CliMA, FuXi, FourCastNet, and AIFS have emerged; however, none support 37-layer pressure level inputs and some of them lack open access, thus excluding them from this research framework.

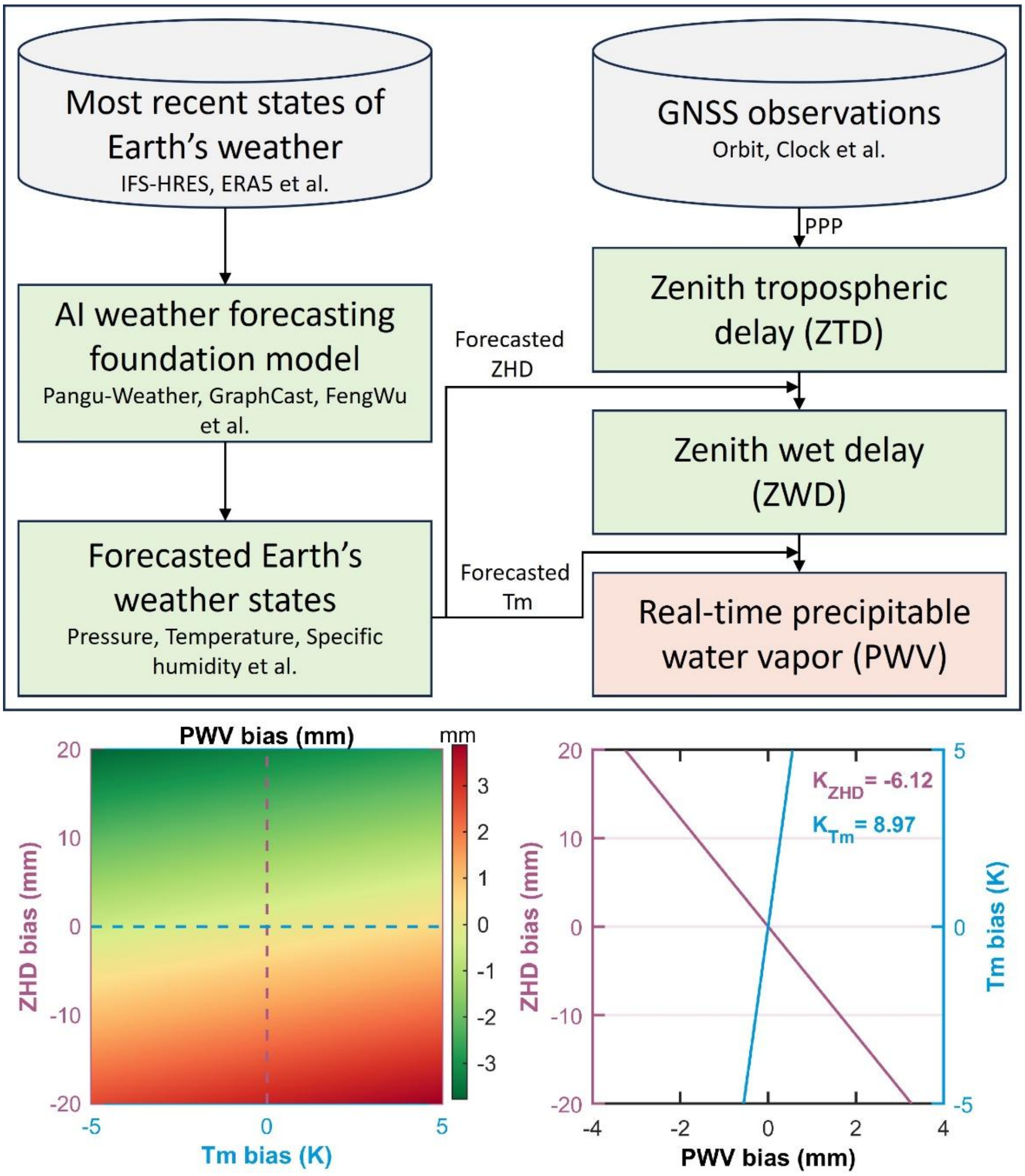

Figure 1. Flowchart of real-time GNSS PWV retrieval system based on AI weather forecasting foundation models and PWV bias caused by ZHD bias and Tm bias. The bottom right panel shows the variation of PWV bias with the variation of Tm bias and ZHD bias for ZHD = 0 and Tm = 0, i.e., the dashed line corresponding to the bottom left panel.

The upper panel of Figure 1 shows the technical flowchart of the proposed real-time GNSS PWV retrieval strategy. The key is to obtain the forecasted ZHD and Tm from the AI foundation models. It meets the needs of converting real-time GNSS tropospheric delays into real-time PWV while avoiding errors introduced by empirical models. The lower panels of Figure 1 show the bias in PWV caused by errors in ZHD and Tm according to Eqs. (1), (4) and (5). The results indicate that a ±6.12 mm ZHD bias or an ±8.97 K Tm bias each leads to a 1 mm PWV bias.

2.3. IGRA2 Radiosonde Data and NGL GNSS Tropospheric Products

Global radiosonde observations from 2022 were utilized as a reference to assess the accuracy of the GNSS PWV under the proposed solution. The radiosonde observations were obtained from the Integrated Global Radiosonde Archive Version 2.2 (*Durre et al., 2018*). We applied stringent quality control to the dataset using the same strategy as *Zhang et al (2019), Zheng et al. (2022) and Yuan et al (2023)*, i.e., (1) records are available at the surface and the top pressure level recorded is at least 300 hPa; (2) there are at least five records of standard pressure levels below (and above) the pressure level of 1000 hPa; and (3) the gap between pressure levels is less than 200 hPa. Given the scarcity of stations in the dataset that fulfill all criteria, experiments included those stations with surface-level data records, enabling the empirical calculation of ZHD and Tm. However, it's important to note that this approach introduces errors from empirical modeling. To investigate this error, we designed experiments and then analyzed them in detail in Section 3.1.

The Nevada Geodetic Laboratory (NGL) provides tropospheric delay products from over 20,000 GNSS stations worldwide, making it the most complete data set of tropospheric delays in the world today. The dataset spans the period from 1994 to the present and provides ZTD, ZWD, gradients and PWV in 5-minute interval. The accuracy of the NGL tropospheric products is comparable to that of the IGS products, making them a reliable reference for evaluating general tropospheric models (*Ding and Chen, 2020*). Note that the NGL strategy uses TU Wien's grid model for ZHD and Tm, which also causes NGL's ZWD and PWV products to include this model error (*Yuan et al., 2021; Ding et al., 2023*). Only NGL's ZTD product is used in our experiments.

As a special note, NGL ZTD is not designed for real-time applications. We selected it for our experiments because our goal is to establish a globally available method for converting GNSS ZTD to high-accuracy PWV in real-time, rather than providing the real-time GNSS PWV products. Therefore, the real-time nature of ZTD does not impact the conclusions drawn in this research. The accuracies mentioned in this research are also relative to those that would be achieved if ERA5 were used for retrospective calculations, representing relative accuracy. Additionally, users can also utilize the forecasted ZHD at the time of GNSS processing (we also recommend that); as the ZHD error will be absorbed by ZWD and have minimal impact on ZTD (*Ding et al., 2023*), this method is essentially equivalent to the one depicted in Figure 1 of this paper.

3. Results and Discussion

In this section, the accuracies of ZHD and Tm computed by the integral method and empirical models at different pressure levels are analyzed first. Then, the RMSEs of ZHD, Tm, and GNSS PWV for the three AI foundation models are obtained and analyzed for the 0-15 day forecast time horizon using ERA5 and co-location radiosonde measurements as references. Finally, the spatial characterization of the accuracy of the global GNSS PWV computed using the three AI foundation models is analyzed.

3.1. Vertical integrals vs. empirical models

The upper panels of Figure 2 (scatter plots) display the RMSEs for ZHD and Tm at over 2,600 radiosonde sites worldwide, derived from empirical models using 13-, 25-, and 37-level ERA5 data, with results from the integral method as reference. We specifically compare the 25-level results here because the VMF forecast products provided by TU Wien, which are based on the 25-level ECMWF products, include ZHD forecasts. It's important to note that VMF lacks Tm data for our study's experiments and its forecasted products can only be used to access previous years' data, with real-time results requiring licensing. The scatter plots in Figure 2 reveal that the ZHD RMSE at 13 pressure levels is notably higher compared to those at 25 and 37 pressure levels. However, the Tm results at 13 pressure levels do not exhibit inferior performance relative to the results of the other two solutions. This is due to the fact that most of the missing pressure levels when using 13 levels are above 50 hPa, where there is almost no water vapor present, resulting in minimal contribution to the calculation of Tm. For ZHD, the error due to the empirical model Saastamoinen is less than 3 mm for the majority of sites when using 25 level or 37 level. Similarly, for Tm, the error due to the empirical Bevis model is less than 4 K for the majority of sites, whether using 13, 25, or 37 levels. Note that in the polar region, it is not recommended to use the Bevis model as it may lead to errors exceeding 10 K.

The lower panels of Figure 2 (box plots) show the results of each solution using the radiosonde observations as a reference. There are only 93 stations that satisfy our requirements for the integration method, most of which are located in the United States (see the small black dots in the $Tm_{13level}$ plot in Figure 2). From the figure, we find that the integration method for the 13-level case yields a ZHD error of about 9 mm, which introducing an error larger than 1 mm to PWV, making it unacceptable. Therefore, we use Saastamoinen to calculate the ZHD under the Pangu-Weather solution in the subsequent experiments. For the other pressure level configurations, the RMSEs of the integral method achieve RMSE values of around 3 mm, while the Saastamoinen methods are all around 5 mm. The difference in Tm between different pressure levels is minimal, with the RMSEs of the integral method are all around 1.6 K, while the RMSEs of the Bevis method are all around 3.5 K. According to the conversion relationship demonstrated in Figure 1, the empirical Saastamoinen model leads to a PWV bias of about 0.3 mm, while the empirical Bevis model leads to a PWV bias of about 0.2 mm.

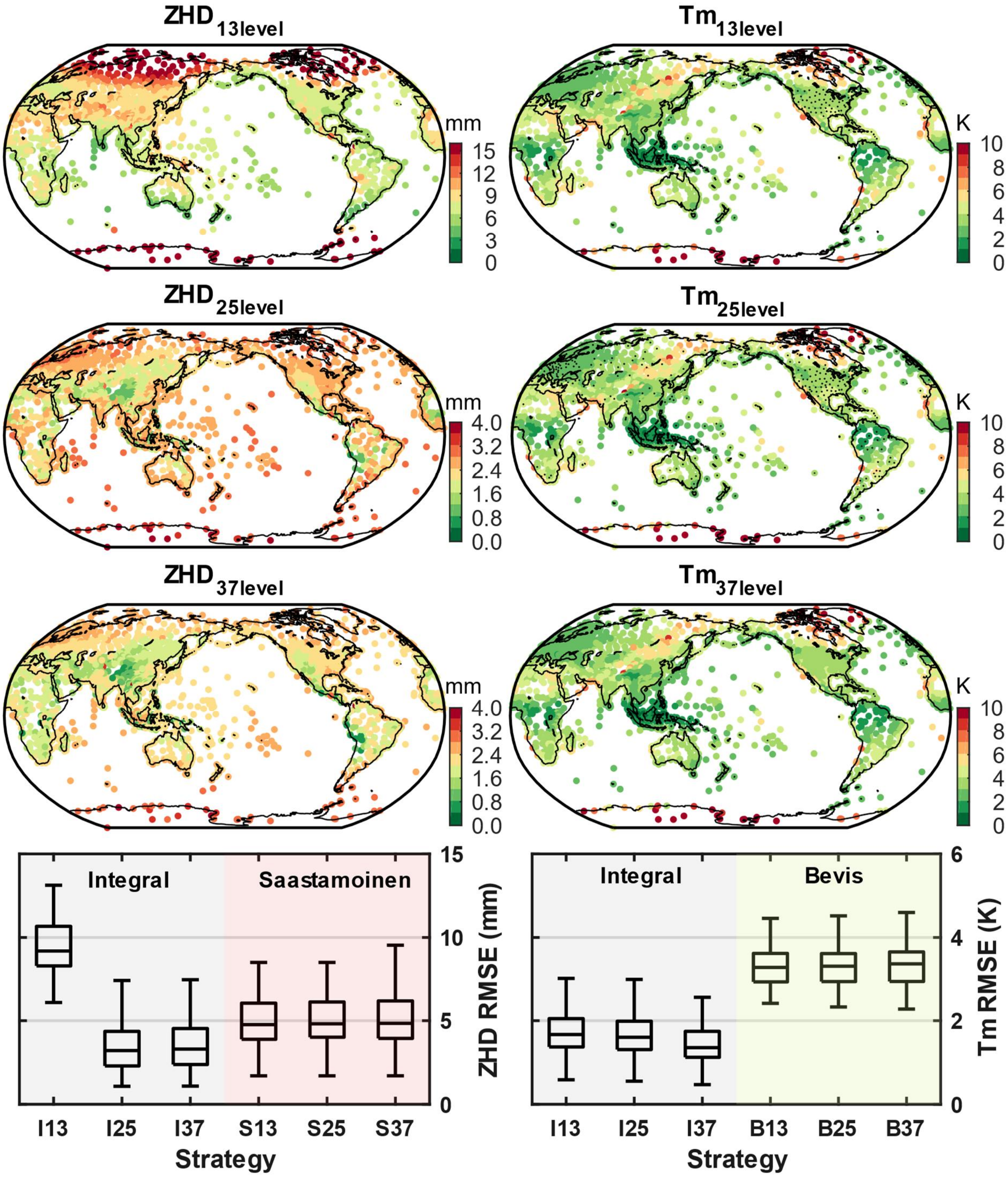

Figure 2. Root-mean-square errors (RMSEs) of zenith hydrostatic delay (ZHD) and weighted mean temperature (Tm) for different strategies (Integral vs. Saastamoinen for ZHD, Integral vs. Bevis for Tm) using ERA5 of 13-, 25-, and 37- pressure levels. The global scatterplots show the comparison between the integral method and the empirical model (Saastamoinen and Bevis), and the box plots show the RMSE of the various strategies using the measured radiosonde data as a reference.

3.2. Accuracy Evaluation

Figure 3 shows the RMSE of ZHD, Tm and GNSS PWV calculated using the 0-15 day forecast results from the Pangu-Weather, GraphCast and FengWu models. The left panels in Figure 3 depict the results of the three AI foundation models for more than 8000 GNSS stations (see Figure 4 for individual stations) using ERA5 as a reference, while the middle panels and the right panels are the results using the co-located radiosonde data as a reference. Note that since there is no perfect (i.e., zero distance) co-located, we define co-location as GNSS stations and radiosondes within 40 km. *Ding and Chen (2021)* discuss the differences between the two sources of PWV as a function of distance, and we follow their definition of co-location. The middle panels are the results for the 93 radiosonde stations that are able to fulfill the requirements of the integration method, and the right panels are the results for the 489 radiosonde stations (see the small black dots in the $Tm_{25level}$ plot in Figure 2) for which the surface data records of the radiosonde stations are valid. Since the integration method cannot be used at these locations, we rely on the empirical model to compute ZHD and Tm. Note that we included the results using the empirical meteorological parameter model GPT3 (*Landskron & Böhm, 2018*) in the comparison as well to have an intuitive reference for the degradation of the accuracy of the AI foundation models with the forecast duration. Note that this empirical model is usually not used to compute the PWVs because of its poor accuracy. If the method of *Zheng et al. (2022)* is applied to this experiment, it is expected to perform similarly to the GPT3 model shown in Figure 3, essentially resembling a horizontal straight line. Of course, its RMSE would be slightly lower than that of GPT3, improving from 2.8 mm to 2.4 mm.

Pangu-Weather results in a significantly worse GNSS PWV accuracy than GraphCast and FengWu because of fewer pressure level layers. The left panels in Figure 3 show that, the PWV error introduced by the AI model error is less than 1 mm for forecasts less than five days ahead. From the middle panels and right panels, we conclude that the PWVs calculated using the results from forecasts shorter than three days are not significantly different under the three AI solutions as well as the ERA5 solution. In addition, in all comparisons, the results of forecasts up to 10 days are better than those of the empirical model GPT3. Finally, we find that the trends of ZHD RMSE and PWV RMSE are very similar in all comparisons because the ZHD error is the primary contributor to the PWV RMSE. The Tm accuracy is generally very high and results in a smaller impact on the PWV RMSE. Combined with the relationship from Figure 1, the contributions of ZHD and Tm are about 80% and 20%, respectively.

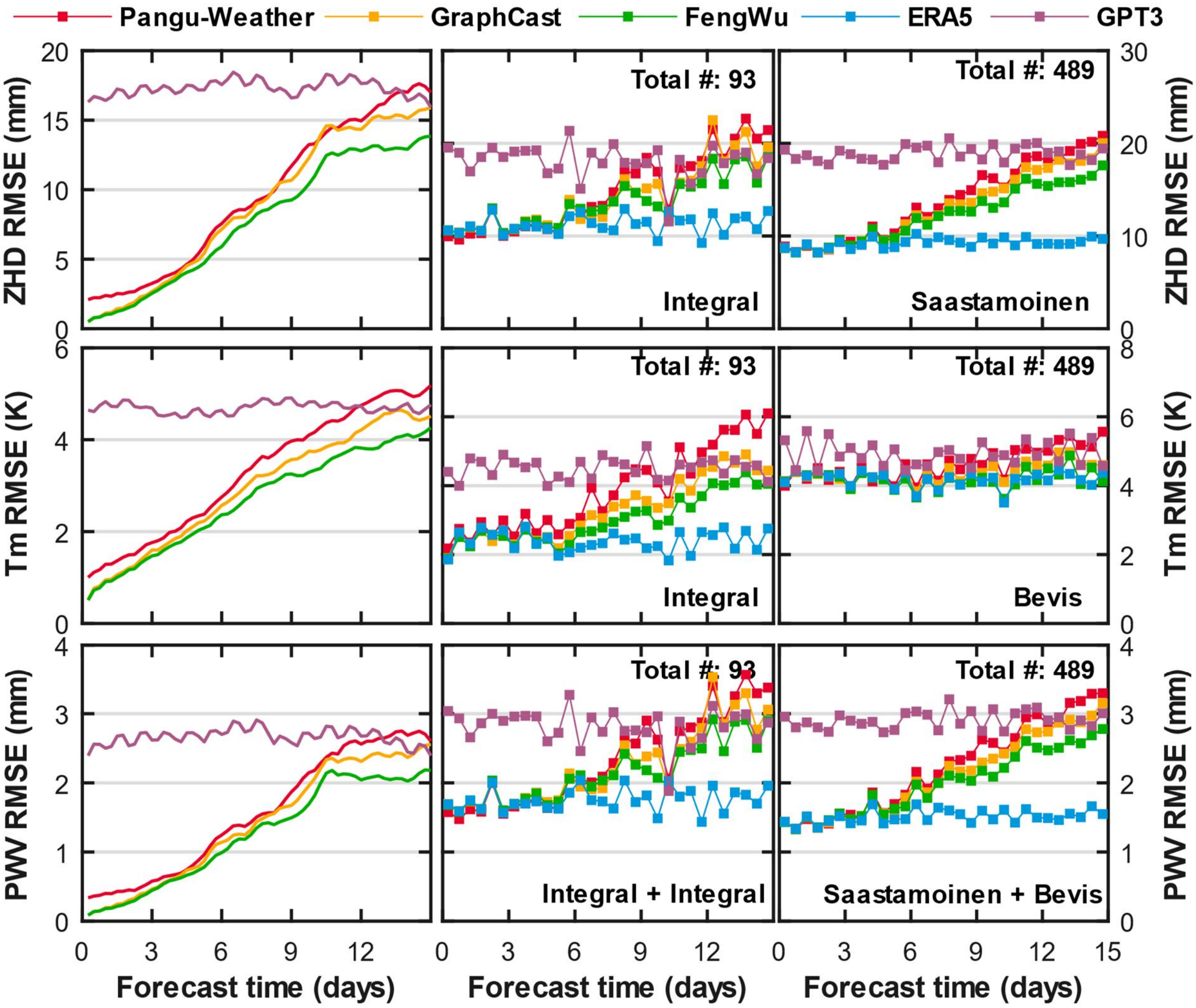

Figure 3. Variation of root-mean-square errors (RMSEs) with forecast time for ZHD, Tm and GNSS PWV. The left panels are the RMSEs referenced to ERA5, and the middle and right panels are the RMSEs referenced to co-located radiosonde observations. Note that all PWVs in the figure are all from GNSS ZTD, and the only differences between the solutions are in the data sources for ZHD and Tm, and in their calculation methods.

3.3. Global GNSS PWV

Based on the results in Figure 3 when using the radiosonde data as a reference, the accuracy of the GNSS PWV computed using the ZHD and Tm within 3 days of the forecast shows very little difference between the three AI solutions, and the difference is barely discernible from the results of using ERA5 Figure 4 shows the RMSEs of 8320 stations for which the NGL GNSS ZTD data record meets the requirements, with forecast durations of 12 hours, 1 day, 2 days, and 3 days, respectively. The upper panels in Figure 4 show the RMSEs for each station, while the lower panels show the average RMSEs at 500 m intervals for different station height intervals. Note that the RMSEs here are calculated using the ERA5 results as a reference, i.e., the same strategy as the left panels in Figure 3.

Among the three AI solutions, GraphCast and FengWu are significantly ahead of Pangu-Weather, while FengWu slightly outperforms GraphCast for all forecast durations. There are two reasons for this result: firstly, Pangu-Weather only supports a maximum of 13 layers of pressure level, which is disadvantageous for accurately expressing the atmospheric state; secondly, the Pangu-Weather solution can only use the empirical model Saastamoinen to calculate the ZHD due to the large error in the integration method for the insufficient number of layers, and this part of the model error is introduced into the calculated PWV. The GNSS PWV accuracies degrade faster in the high-latitude region as the forecast duration increases. Moreover, the GNSS PWV accuracies degrade faster at the edge of continents, especially in narrow peninsulas or archipelagic regions, such as the Antarctic Peninsula, the Aleutian Islands, and the Newfoundland Islands region of Canandaigua, among others. The former may be caused by the lower accuracy of ZHD in high latitude regions, while the latter may be caused by the sharp fluctuation of water vapor and the decrease in the accuracy of Tm. In terms of the change of PWV RMSE with height, overall, the PWV accuracy becomes higher with increasing station height, which is because the value of PWV itself also decreases with increasing height. In addition, the difference between the results of Pangu-Weather and the other two solutions becomes smaller as the forecast length increases, as well as the height increases. In contrast, the difference between the results of GraphCast and FengWu solutions is gets larger as the height increases.

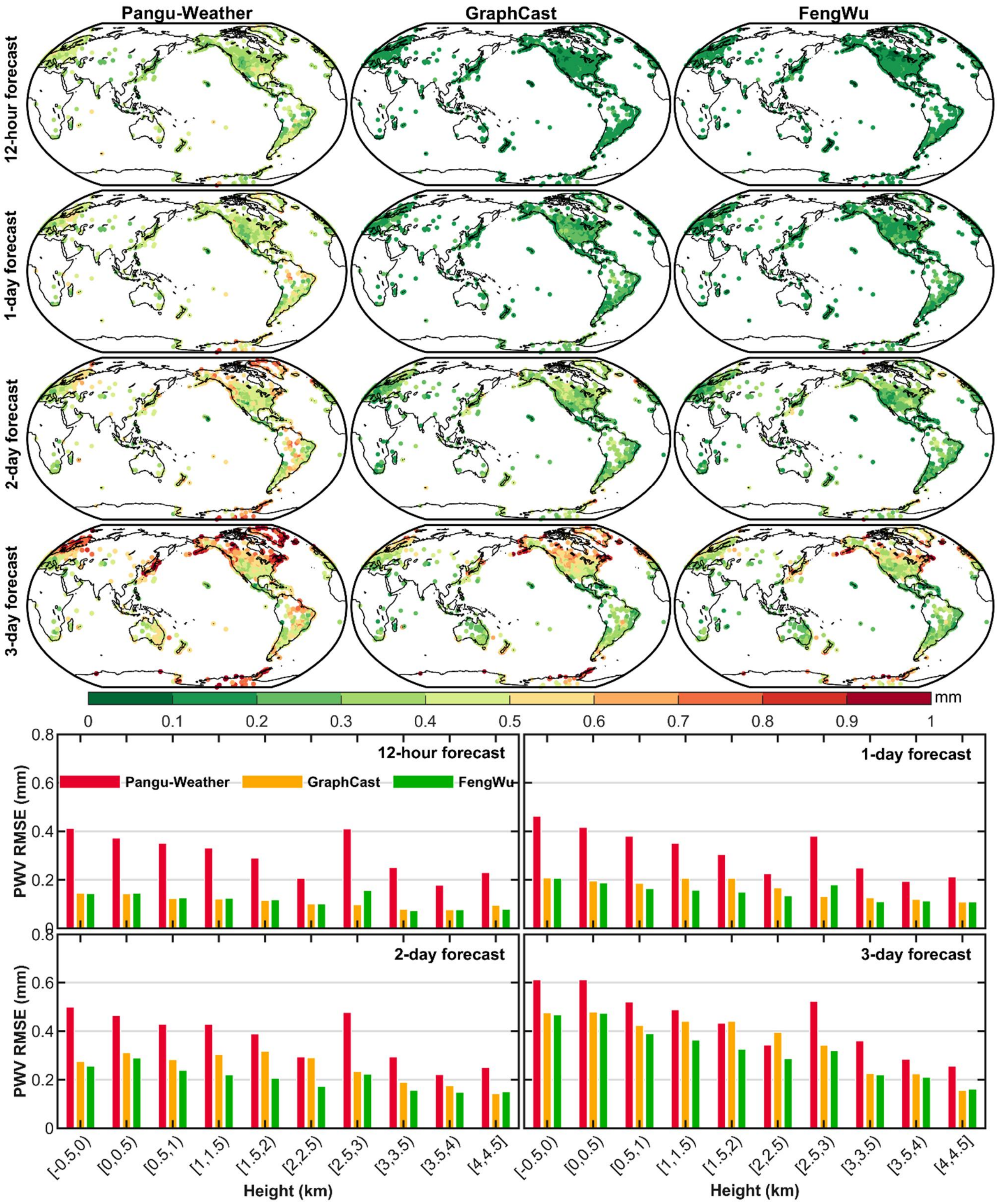

Figure 4. Root-mean-square errors (RMSEs) of global GNSS PWV derived from three AI foundation models w.r.t. to GNSS PWV using ERA5. The upper panels show the RMSEs of global GNSS sites for 12-hour, 1-day, 2-day, and 3-day forecasts for the three solutions, respectively. The lower panels show the RMSEs according to height partitioning under the same forecast durations.

4. Conclusions

We presented a novel method to retrieve highly accurate real-time PWV from GNSS tropospheric delay based on AI weather forecast foundation models. In this method, the forecasted atmospheric state is firstly obtained by using foundation models such as Pangu-Weather, GraphCast, and FengWu, then the integral ZHD and integral Tm are computed from the forecasted atmospheric state, and finally, the high-precision real-time GNSS PWV is obtained from the real-time GNSS ZTD. Compared to conventional approaches, our method boasts three key benefits: (1) It enables the creation of pressure level atmospheric states at any global location directly on the user's computing device, thereby meeting the need for instantaneous PWV retrieval within seconds; (2) The atmospheric state produced is compatible with the integral method for calculating ZHD and Tm, circumventing the inaccuracies associated with empirical models (the compounded error from two empirical models could lead to a PWV RMSE of up to 0.5 mm); (3) This method ensures that the real-time GNSS PWV as close as possible to the results obtained through post-processing with reanalyzed NWM, thereby avoiding the inaccuracies introduced by varying spatial distances and the use of imperfectly co-located radiosonde observations. Of the three AI solutions, FengWu performs the best, followed by GraphCast, both of which are substantially ahead of Pangu-Weather. The PWV errors due to ZHD and Tm calculated using forecasts shorter than 3 days are not significantly different from the post-processed PWV errors calculated using ERA5 results. The PWV errors introduced by the AI-based forecasts are typically less than 1 mm when calculated using forecasts less than 5 days ahead.

The proposed method has the potential to significantly contribute to atmospheric monitoring significantly by providing high-accuracy forecasted ZHD and Tm for real-time GNSS PWV retrieval at any global position within seconds, ensuring a precision loss of GNSS PWV within 0.1 mm (6-hour forecast) due to incorrect ZHD and Tm. This will enable the global network of dense GNSS stations to offer reliable and timely PWV for weather disaster prediction and alerts. We recommend substituting the traditional GNSS PWV retrieval from ZTD with this novel method to preserve GNSS technology's edge in delivering real-time products with minimal accuracy degradation. It is crucial to emphasize the significance of utilizing a highly accurate NWM for the initial epoch inference of the AI forecast model, as employing a lower accuracy NWM could result in cumulative errors in the final PWV.

Data Availability Statement

This research processed data from more than 20 TB. The ERA5 data on pressure levels (*Hersbach et al., 2018a*) and ERA5 data on single levels (*Hersbach et al., 2018b*) are available at Copernicus Climate Change Service (C3S) Climate Data Store (CDS) (last accessed 8 Oct, 2023). The NGL GNSS tropospheric delay products are available at http://geodesy.unr.edu/gps_timeseries/trop/ (*Blewitt et al., 2018*). The radiosonde data is available at https://www.ncei.noaa.gov/products/weather-balloon/integrated-global-radiosonde-archive (*Durre et al., 2018*). The foundation model Pangu-Weather is available at https://github.com/198808xc/Pangu-Weather (*Bi et al., 2023*). The foundation model GraphCast is available at https://github.com/google-deepmind/graphcast (*Lam et al., 2023*). The foundation model FengWu is available at https://github.com/OpenEarthLab/FengWu (*Chen et al., 2023*).

Acknowledgments

The authors would like to thank the Technische Universität Wien for the open-source ray-tracing software RADIATE (https://github.com/TUW-VieVS/RADIATE, *Hofmeister 2016*) and ecmwf-lab for open-source AI models command-line management tool ai-models (https://github.com/ecmwf-lab/ai-models). This study is financially supported by the General Research Fund of Hong Kong (Grant No. 15229622), the Innovation and Technology Fund of Hong Kong (Grant No. ITP/019/22LP), the National Natural Science Foundation of China (No.11673050) and the National Key R&D Program of China (No. 2018YFB0504300).

References

Adams, D. K., Gutman, S. I., Holub, K. L., & Pereira, D. S. (2013). GNSS observations of deep convective time scales in the Amazon. *Geophysical Research Letters*, 40(11), 2818-2823. https://doi.org/10.1002/grl.50573

Bevis, M., Businger, S., Herring, T. A., Rocken, C., Anthes, R. A., & Ware, R. H. (1992). GPS meteorology: Remote sensing of atmospheric water vapor using the global positioning system. *Journal of Geophysical Research: Atmospheres*, 97(D14), 15787-15801. https://doi.org/10.1029/92JD01517

Bi, K., Xie, L., Zhang, H., Chen, X., Gu, X., & Tian, Q. (2023). Accurate medium-range global weather forecasting with 3D neural networks. *Nature*, 619(7970), 533-538. https://doi.org/10.1038/s41586-023-06185-3

Blewitt, G., & Hammond, W. (2018). Harnessing the GPS data explosion for interdisciplinary science. *Eos*, 99. https://doi.org/10.1029/2018EO104623

Chen, K., Han, T., Gong, J., Bai, L., Ling, F., Luo, J. J., ... & Ouyang, W. (2023). FengWu: Pushing the Skillful Global Medium-range Weather Forecast beyond 10 Days Lead. *arXiv preprint arXiv*:2304.02948. https://doi.org/10.48550/arXiv.2304.02948

Ding, J., & Chen, J. (2020). Assessment of empirical troposphere model GPT3 based on NGL's global troposphere products. *Sensors*, 20(13), 3631. https://doi.org/10.3390/s20133631

Ding, J., & Chen, J. (2021). Accuracy Variability of GNSS PWV in the Range of Small and Medium Scale Areas. *Proceedings of the 12th Annual China Satellite Navigation Conference* - S01 Satellite Navigation Industry Applications.

Ding, J., Chen, J., Tang, W., & Song, Z. (2022a). Spatial–Temporal Variability of Global GNSS-Derived Precipitable Water Vapor (1994–2020) and Climate Implications. *Remote Sensing*, 14(14), 3493. https://doi.org/10.3390/rs14143493

Ding, J., Chen, J., & Tang, W. (2022b). Increasing Trend of Precipitable Water Vapor in Antarctica and Greenland. *In China Satellite Navigation Conference (pp. 286-296)*. Singapore: Springer Nature Singapore. https://doi.org/10.1007/978-981-19-2588-7_27

Ding, J., Chen, J., Wang, J., & Zhang, Y. (2023). Characteristic differences in tropospheric delay between Nevada Geodetic Laboratory products and NWM ray-tracing. *GPS Solutions*, 27(1), 47. https://doi.org/10.1007/s10291-022-01385-2

Ding, W., Teferle, F. N., Kazmierski, K., Laurichesse, D., & Yuan, Y. (2017). An evaluation of real-time troposphere estimation based on GNSS Precise Point Positioning. *Journal of Geophysical Research: Atmospheres*, 122(5), 2779-2790. https://doi.org/10.1002/2016JD025727

Durre, I., Yin, X., Vose, R. S., Applequist, S., & Arnfield, J. (2018). Enhancing the data coverage in the Integrated Global Radiosonde Archive. *Journal of Atmospheric and Oceanic Technology*, 35(9), 1753-1770. https://doi.org/10.1175/JTECH-D-17-0223.1

Ejigu, Y. G., Teferle, F. N., Klos, A., Bogusz, J., & Hunegnaw, A. (2021). Monitoring and prediction of hurricane tracks using GPS tropospheric products. *GPS Solutions*, 25(2), 76. https://doi.org/10.1007/s10291-021-01104-3

Guo, A., Xu, Y., Jiang, N., Wu, Y., Gao, Z., Li, S., ... & Bastos, L. (2023). Analyzing correlations between GNSS retrieved precipitable water vapor and land surface temperature after earthquakes occurrence. *Science of The Total Environment*, 872, 162225. https://doi.org/10.1016/j.scitotenv.2023.162225

Hersbach, H., Bell, B., Berrisford, P., Biavati, G., Horányi, A., Muñoz Sabater, J., ... & Thépaut, J. N. (2018a). ERA5 hourly data on pressure levels from 1979 to present. *Copernicus climate change service (c3s) climate data store (cds)*, 10(10.24381). doi: 10.24381/cds.bd0915c6.

Hersbach, H., Bell, B., Berrisford, P., Biavati, G., Horányi, A., Muñoz Sabater, J., ... & Thépaut, J. N. (2018b). ERA5 hourly data on single levels from 1979 to present. *Copernicus climate change service (c3s) climate data store (cds)*, 10(10.24381). doi: 10.24381/cds.adbb2d47.

Hofmeister, A. (2016). Determination of path delays in the atmosphere for geodetic VLBI by means of ray-tracing. http://hdl.handle.net/20.500.12708/136

Huang, L., Mo, Z., Xie, S., Liu, L., Chen, J., Kang, C., & Wang, S. (2021). Spatiotemporal characteristics of GNSS-derived precipitable water vapor during heavy rainfall events in Guilin, China. *Satellite Navigation*, 2, 1-17. https://doi.org/10.1186/s43020-021-00046-y

Jade, S., & Vijayan, M. S. M. (2008). GPS-based atmospheric precipitable water vapor estimation using meteorological parameters interpolated from NCEP global reanalysis data. *Journal of Geophysical Research: Atmospheres*, 113(D3). https://doi.org/10.1029/2007JD008758

Jiang, N., Wu, Y., Li, S., Xu, Y., Wang, Y., & Xu, T. (2024). First PWV retrieval using MERSI-LL onboard FY-3E and cross validation with co-platform occultation and ground GNSS. *Geophysical Research Letters*, 51(8), e2024GL108681. https://doi.org/10.1029/2024GL108681

Lam, R., Sanchez-Gonzalez, A., Willson, M., Wirnsberger, P., Fortunato, M., Alet, F., ... & Battaglia, P. (2023). Learning skillful medium-range global weather forecasting. *Science*, eadi2336. https://doi.org/10.1126/science.adi2336

Landskron, D., & Böhm, J. (2018). VMF3/GPT3: refined discrete and empirical troposphere mapping functions. *Journal of Geodesy*, 92, 349-360. https://doi.org/10.1007/s00190-017-1066-2

Li, X., Tan, H., Li, X., Dick, G., Wickert, J., & Schuh, H. (2018). Real-Time Sensing of Precipitable Water Vapor from BeiDou Observations: Hong Kong and CMONOC Networks. *Journal of Geophysical Research: Atmospheres*, 123(15), 7897-7909. https://doi.org/10.1029/2018JD028320

Ma, X., Yao, Y., Zhang, B., & He, C. (2022). Retrieval of high spatial resolution precipitable water vapor maps using heterogeneous earth observation data. *Remote Sensing of Environment*, 278, 113100. https://doi.org/10.1016/j.rse.2022.113100

Miranda, P. M. A., Adams, D. K., Tomé, R., Fernandes, R., & Mateus, P. (2023). Optimizing Boundary Conditions in GNSS Tomography: A Continuous 7-Month Case Study in the Amazon. *Geophysical Research Letters*, 50(22), e2023GL105030. https://doi.org/10.1029/2023GL105030

Rocken, C., Van Hove, T., & Ware, R. (1997). Near real-time GPS sensing of atmospheric water vapor. *Geophysical research letters*, 24(24), 3221-3224. https://doi.org/10.1029/97GL03312

Saastamoinen, J. (1972). Atmospheric correction for the troposphere and stratosphere in radio ranging satellites. *The use of Artificial Satellites for Geodesy*, 15, 247-251. https://doi.org/10.1029/GM015p0247

Vaquero-Martínez, J., Antón, M., de Galisteo, J. P. O., Román, R., Cachorro, V. E., & Mateos, D. (2019). Comparison of integrated water vapor from GNSS and radiosounding at four GRUAN stations. *Science of the total environment*, 648, 1639-1648. https://doi.org/10.1016/j.scitotenv.2018.08.192

Wang, J., Wu, Z., Semmling, M., Zus, F., Gerland, S., Ramatschi, M., ... & Schuh, H. (2019). Retrieving precipitable water vapor from shipborne multi-GNSS observations. *Geophysical Research Letters*, 46(9), 5000-5008. https://doi.org/10.1029/2019GL082136

Wang, J., Zhang, L., Dai, A., Van Hove, T., & Van Baelen, J. (2007). A near-global, 2-hourly data set of atmospheric precipitable water from ground-based GPS measurements. *Journal of Geophysical Research: Atmospheres*, 112(D11). https://doi.org/10.1029/2006JD007529

Wang, X., Zhang, K., Wu, S., Li, Z., Cheng, Y., Li, L., & Yuan, H. (2018). The correlation between GNSS-derived precipitable water vapor and sea surface temperature and its responses to El Niño–Southern Oscillation. *Remote sensing of environment*, 216, 1-12. https://doi.org/10.1016/j.rse.2018.06.029

Wei, J., Shu, Y., Liu, Y., Fang, R., Qiao, L., Ding, D., ... & Liu, J. (2023). Retrieving Accurate Precipitable Water Vapor Based on GNSS Multi-Antenna PPP With an Ocean-Based Dynamic Experiment. *Geophysical Research Letters*, 50(6), e2023GL102982. https://doi.org/10.1029/2023GL102982

Wu, Z., Lu, C., Han, X., Zheng, Y., Wang, B., Wang, J., ... & Liu, Y. (2023). Real-time shipborne multi-

GNSS atmospheric water vapor retrieval over the South China Sea. *GPS Solutions*, 27(4), 179. https://doi.org/10.1007/s10291-023-01519-0

Yu, C., Penna, N. T., & Li, Z. (2017). Generation of real-time mode high-resolution water vapor fields from GPS observations. *Journal of Geophysical Research: Atmospheres*, 122(3), 2008-2025. https://doi.org/10.1002/2016JD025753

Yuan, P., Blewitt, G., Kreemer, C., Hammond, W. C., Argus, D., Yin, X., ... & Kutterer, H. (2023). An enhanced integrated water vapour dataset from more than 10,000 global ground-based GPS stations in 2020. *Earth System Science Data*, 15, 723–743. https://doi.org/10.5194/essd-15-723-2023

Yuan, P., Hunegnaw, A., Alshawaf, F., Awange, J., Klos, A., Teferle, F. N., & Kutterer, H. (2021). Feasibility of ERA5 integrated water vapor trends for climate change analysis in continental Europe: An evaluation with GPS (1994–2019) by considering statistical significance. *Remote Sensing of Environment*, 260, 112416. https://doi.org/10.1016/j.rse.2021.112416

Yuan, Y., Zhang, K., Rohm, W., Choy, S., Norman, R., & Wang, C. S. (2014). Real-time retrieval of precipitable water vapor from GPS precise point positioning. *Journal of geophysical research: atmospheres*, 119(16), 10044-10057. https://doi.org/10.1002/2014JD021486

Zhao, Q., Liu, Y., Ma, X., Yao, W., Yao, Y., & Li, X. (2020). An improved rainfall forecasting model based on GNSS observations. *IEEE Transactions on Geoscience and Remote Sensing*, 58(7), 4891-4900. https://doi.org/10.1109/TGRS.2020.2968124

Zhang, W., Lou, Y., Cao, Y., Liang, H., Shi, C., Huang, J., ... & Fan, B. (2019). Corrections of radiosonde-based precipitable water using ground-based GPS and applications on historical radiosonde data over China. *Journal of Geophysical Research: Atmospheres*, 124(6), 3208-3222. https://doi.org/10.1029/2018JD029662

Zheng, Y., Lu, C., Wu, Z., Liao, J., Zhang, Y., & Wang, Q. (2022). Machine Learning-Based Model for Real-Time GNSS Precipitable Water Vapor Sensing. *Geophysical Research Letters*, 49(3), e2021GL096408. https://doi.org/10.1029/2021GL096408

Zhu, H., Chen, K., Chai, H., Ye, Y., & Liu, W. (2024). Characterizing extreme drought and wetness in Guangdong, China using global navigation satellite system and precipitation data. *Satellite Navigation*, 5(1), 1. https://doi.org/10.1186/s43020-023-00121-6